Nonlinear Analysis: Modelling and Control, 2006, Vol. 11, No. 4, 345–365

Theoretical Modeling and Optimization of the Detection Performance: a New Concept for Electrochemical Detection of Proteins in Microfluidic Channels

C. Amatore[1], **A. Oleinick**[1,2], **I. Svir**[2], **N. da Mota**[1], **L. Thouin**[1]

[1]Ecole Normale Superieure, Department de Chimie,
UMR CNRS 8640 "PASTEUR"
24 rue Lhomond, 75231 Paris Cedex 05, France
christian.amatore@ens.fr

[2]Kharkov National University of Radioelectronics
Mathematical and Computer Modelling Laboratory
14 Lenin Avenue, Kharkov, 61166, Ukraine
irina.svir@kture.kharkov.ua

Received: 04.08.2006 **Revised:** 09.10.2006 **Published online:** 30.10.2006

Abstract. In this work, we present a complete theoretical analysis of a new concept of electrochemical detector for application in proteomics upon considering two band microelectrodes performing in generator-collector mode. This concept of an original electrochemical detector is aimed at the detection of proteins following their separation in microfluidic biochips. The theoretical analysis is based on the use of the time-dependent coordinate transformation which allows performing precise modeling for a wide range of the key parameters governing the electrochemical detector performance. This allows defining a precise optimization procedure for its best efficiency upon considering the qualitative and quantitative effects of each of the main operational parameters.

Keywords: computational electrochemistry, electrochemical detector, lab-on-a-chip, microchannel, microfluidics.

1 Introduction

The principle of miniaturized separation and detection of biological samples and fluids is nowadays extended to a broad variety of situations, especially for ap-

plication in proteomics. Then discrete samples of cell extracts may be treated, separated and then analyzed through microfluidic systems. When considering proteomics, *stricto sensu*, the aim is to elaborate a proteic cartography of specific cells and tissues. Henceforth, this requires high throughput rates coupled with coupling to protein structural analysis. For these reasons, proteomic biochips are generally used in association with electrospray ionization mass spectrometry, which solves the problem of detection and characterization of separated proteins [1].

Another desirable application of microfluidic systems with respect to applications deriving from proteomics consists in developing portable devices which will be specialized in monitoring a few specific proteins and their relative population in a fluid extract for medical diagnostic or food quality control. If the size of the overall device, including the detection component, may be sufficiently miniaturized and produced with disposable materials to avoid inter-sample contamination, such devices may indeed perform out of sophisticated laboratories and therefore may be used in future on routine basis for medical checking and prevention purposes in hospitals, doctors' offices, or for quality control, e.g. in food processing units [2].

Evidently, the integration of the sample treatment and separation units on microchips will not differ basically from what is now used in proteomics, except that they will be focused onto the separation of only a few target proteins. These are standard technologies today [3]. The problem of designing a cheap, easy-to-operate and portable/disposable device thus relies only onto the ability to produce precise but technologically simple detection units which may be connected to the end of the separation channel on the chip.

In this context it seems that electrochemistry is a method of choice if it can be adapted to protein detection within microfluidic assemblies. Indeed, this is a particularly adapted method since electrochemical currents are proportional to concentrations, and concentrations are always maintained high in microfluidic systems even when quantities are extremely small. Furthermore, electrochemical devices may be driven and operated with cheap and portable instrumentations (e.g., PDAs). However, two main issues prevent a direct application of electrochemical methods for protein detection in microfluidic chips. The first one is that proteins give often sluggish electrochemical signals and frequently this occurs

though adsorption onto electrodes [4]. The second is that proteins are generally large molecules whose diffusivities are extremely low. This implies that a direct electrochemical sensor in a microfluidic channel will produce weak and hardly reliable electrochemical signals, and moreover will probe only the fraction of proteins transiting near the channel wall in which the electrode is embedded, i.e., in the very region where the separation is not representative since it may be altered by any interaction between the wall and the flow or the protein sample.

We wish to examine here an electrochemical concept which overcomes both limitations without introducing significant difficulties in the microfabrication processes of the electrodes-channel assembly or in the detection. This is based on an adequate use of the extreme intrinsic sensitivity of generator-collector devices to kinetics.

The operation of simple electrochemical generator-collector assemblies operating in microfluidic channels (see Fig. 1(a)) have been recently investigated in our laboratories and by others [5–8]. Basically, this consists in electrogenerating a mediator, viz. an activated species, M, by reduction or oxidation of its inert precursor, A, at the upstream generator electrode. Species M travels by diffusion across over the whole channel height while being carried by the hydrodynamic convection along the channel flow. It may then be detected by a collector electrode placed downstream. Whenever, M is stable chemically, viz. in absence of protein its resting steady state current at the collector measured relative to the steady state current at the generator is a constant which depends on the geometric configuration, diffusion coefficients and the local flow hydrodynamics. Let us posit $\phi^0_{coll} = (i_{coll}/i_{gen})^0$ be this constant, the superscript "0" indicating that M experiences no kinetic decay during its time-of-flight in between the two electrodes.

Let us now suppose that M is a species prone to react with proteins, while its precursor A is nonreacting. When a wave of protein (i.e., as resulting from the operation of the upstream separation component of the chip), paves in front of detector, a significant fraction of M will react as a function of the protein transit time in between the generator and collector and of its reactivity. Thus ϕ_{coll} decays. As soon as what remains of the protein wave has passed beyond the collector, the concentration of M is restored to its value in the absence of protein. Then, one

has again $\phi_{coll} = \phi^0_{coll}$. Therefore, one sees that ϕ_{coll} variation with time tracks the passage of a protein wave in front of the detection assembly.

Implementation of this principle requires nevertheless the resolution of several constraints. One is the chemical duality of A/M vs. their reaction towards proteins. Many redox couples maybe thought of, for example, A being a catechol and M its associated quinone (viz., involving a classical "$-2e-2H+$" oxidative process at the generator) since this has been already reported to be an efficient method for protein tagging in microfluidic channels to facilitate their mass spectroscopic detection [9, 10]. The only serious difficulty related to our concept validation is then associated with controlling the kinetic and electrochemical properties of the detection assembly. Indeed, to offer some experimental interest for the detection and quantification of a few protein populations, the time variation of the collection efficiency $\phi_{coll}(t)$ must track as accurately as possible the shape and magnitude of the protein wave as it is produced by the upstream separation compartment.

Besides introducing the above original concept, it is the purpose of this work to investigate and solve theoretically the problem of its optimization.

2 Theory

A double band flow channel generator-collector system is described by many parameters which all formally contribute to determine its general behavior and its efficiency, yet not to the same extent. This is the primary reason for elaborating a simplified model, which preserves all of the main kinetic and electrochemical features of the system at hand and provides therefore a general means of analysis of such systems.

2.1 Delineation and formulation of the problem

First of all, we note that due to the structure of proteins, which usually prevents the reactants from easy access to the reaction sites, the rate constants of the chemical step of chemical modification of proteins are generally small [10]. This fact implies that "the time of flight" of the electrogenerated reactant should generally be sufficiently long to allow its significant decay due to homogeneous reaction with the protein. In turn this implies a long reaction chamber into the channel,

where “long” refers to the channel height and generator/collector band electrode widths. In the case of a sufficiently long channel we have previously shown that at steady state the reactant concentration distribution downstream from the generator is homogeneous across the channel above some distance, L_{down}, (Fig. 1(a), (b)) which may be estimated as [11]:

$$L_{down} = Pe - W + 4, \tag{1}$$

where $W = w/h$ is the dimensionless width of the band, $Pe = vh/D$ is the Péclet number, w is the width of the microband electrode, v is the characteristic linear flow velocity, h is the height of the channel, D is the common diffusion coefficient of the mediator electroactive couple (viz., the electrogenerated reactant and its precursor).

When the precursor flux before the generator is constant, this homogeneous zone extends unaffected downstream along the channel until it meets the diffusion field zone created by the collector electrode. By reciprocity of what occurs at the generator, the latter extends up to a distance L_{up} in the upstream direction from the upstream collector edge.

Thus the microfluidic detector can be divided into three compartments (Fig. 1(a)). The first one is the compartment including the space located upstream of the generator and the space downstream of it where concentration distributions are not homogenous, i.e. over the distance L_{down} from the downstream generator edge (Fig. 1(b)). The second compartment, of length L, is the compartment located in between the two electrodes where no concentration gradient exists along the height of the channel when the system performs under steady-state. The third one is the collector compartment where concentration distributions are again non-uniform; this begins at the distance L_{up} from to the collector electrode upstream edge.

As was said above, owing to the low reactivity of proteins, the length of the second compartment, viz. the reaction kinetic chamber, needs to be much larger than $L_{up} + L_{down}$, possibly by two or three orders of magnitude. This implies that computing the overall behavior of the whole system using finite differences on a uniform grid would be prohibitive in terms of computational time and storage memory whenever sufficient precision is required. For the effective treatment of the problem at hand we thus propose to consider separately each of the three

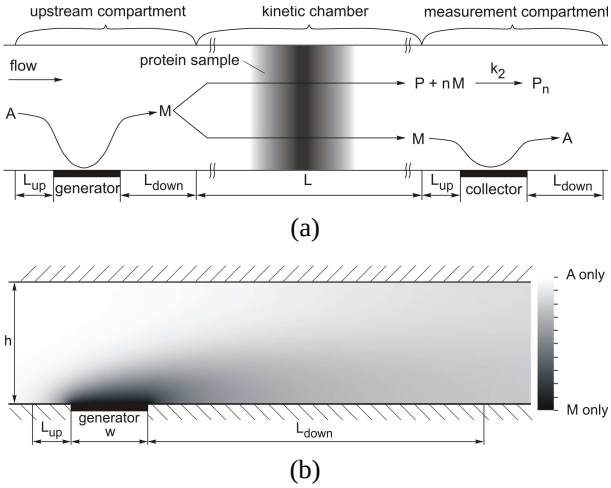

Fig. 1. Schematic representation of the microfluidic generator-collector assembly for protein (P) detection. (a) Device overview indicating the three compartments and its working principle. (b) Expanded view of the generator compartment showing the concentration distribution of the mediator (M) and its precursor (A).

zones delineated above and recombine them sequentially afterwards in order to reconstruct the whole behavior of the system. The behavior of the generator and collector compartments are easily simulated using the conformal mapping approach previously described [12] or any other appropriate simulation approach, for example [13–16].

In this work, we will therefore focus onto the reaction kinetic chamber (homogeneous compartment, see Fig. 1(a)) and model the corresponding mediator-protein kinetics in this zone, since this is the key to the detector performance.

One expects the optimal performing conditions of the system to involve not very high Péclet numbers (see below) since low kinetics requires a sufficiently long time of flight of the species between the generator and collector electrodes. This means that in the kinetic chamber the concentration profiles may tend to homogenize laterally by diffusion (i.e., along the axis of the flow). This fact obviously creates a difficult situation for precise detection, since this amounts to broadening progressively the spatial perturbation which provokes ϕ_{coll} to be different from ϕ^0_{coll}. Overcoming this difficulty requires a detailed analysis and optimization of the device parameters which we present in this work.

Four non-detrimental assumptions have been made for simplification of our model presentation.

First, we assume that the solution velocity profile is constant along the height of the channel. It is known that in pressure-driven channel systems the velocity profile should be parabolic [17, 18] or at least parabolic-like [19, 20]. However, for electroosmotic-driven flows this assumption is realistic. Furthermore, even if computed characteristics of the response will depend on the exact flow shape, the main trends of the system which are crucial to understand its behavior will remain unaffected.

Second, we consider that the wave of protein approaches the homogeneous compartment of the channel unaffected by its reaction with the mediator species, which is tantamount to considering that $L >> L_{down}$.

Third, we consider here an initial staircase protein sample since this enables to evaluate the result for any other sample shape by virtue of the Fourier transform.

The final assumption concerns the mediator-protein kinetics. Proteins may offer several (n) reaction sites vulnerable to a given mediator [10], so that the overall reaction for a single protein molecule may be viewed as the general following sequence:

$$P + M \xrightarrow{k_1^*} P_1; \quad P_1 + M \xrightarrow{k_2^*} P_2; \quad \ldots; \quad P_{n-1} + M \xrightarrow{k_n^*} P_n, \tag{2}$$

where P denotes the protein molecule; P_i is the protein molecule with i of its n possible reaction sites occupied, and k_i^* are the second order rate constants of the corresponding reaction steps (these may have different values). Applying the kinetic steady-state approximation shows that the reaction sequence (2) can be approximated by a single reaction (Fig. 1):

$$P + nM \xrightarrow{k_2} P_n, \tag{3}$$

where k_2 is an effective second order rate constant and n an effective stoichiometric number. We term both kinetic parameters as "effective" since they are not absolute features of the reaction at hand but depend also on the residence time of the protein and mediator within the kinetic chamber of the channel. The rate of change of the mediator concentration is then

$$\left(\frac{\partial c_m}{\partial t}\right)_{kin} = -nk_2 c_m c_p, \tag{4}$$

while that of the protein concentration is

$$\left(\frac{\partial c_p}{\partial t}\right)_{kin} = -k_2 c_m c_p, \tag{5}$$

where c_m and c_p are the concentrations of the mediator and protein respectively.

2.2 Mathematical model

Taking into account all of the above assumptions we consider now the mathematical model of the homogeneous compartment (see Fig. 1(a)) of the microfluidic system in one dimension, x, along the flow in the channel:

$$\begin{aligned} \frac{\partial c_m}{\partial t} &= D_m \frac{\partial^2 c_m}{\partial x^2} - v_x \frac{\partial c_m}{\partial x} - n k_2 c_m c_p; \\ \frac{\partial c_p}{\partial t} &= D_p \frac{\partial^2 c_p}{\partial x^2} - v_x \frac{\partial c_p}{\partial x} - k_2 c_m c_p, \end{aligned} \tag{6}$$

where D_m and D_p are the diffusion coefficients of the mediator and protein respectively, v_x is the linear velocity of the solution along the flow axis x and t is the time coordinate.

The initial and boundary conditions over the vertically homogeneous section of the channel are:

$$\begin{aligned} t = 0\colon \quad & \forall x, && c_m = c_m^0; \\ & x \notin \left[-\frac{d}{2};\ \frac{d}{2}\right], && c_p = 0; \\ & -\frac{d}{2} \le x \le \frac{d}{2}, && c_p = c_p^0; \\ t > 0\colon \quad & x \to -\infty, && c_m \to c_m^0;\ c_p \to 0; \\ & x \to \infty, && c_m \to c_m^0;\ c_p \to 0, \end{aligned} \tag{7}$$

where d is the width of the protein sample injection (see Fig. 1(a)), the origin of the space x being located at the centre of the protein sample at $t = 0$; c_m^0 is the entrance concentration of the mediator within the channel, c_p^0 is that of the protein sample.

Using the following dimensionless parameters and variables:

$$\begin{aligned} &X = \frac{x}{L};\ \ \tau = \frac{v_x t}{L};\ \ C_m = \frac{c_m}{c_m^0};\ \ C_p = \frac{c_p}{c_m^0};\ \ \gamma = \frac{c_p^0}{c_m^0};\\ &Pe_m = \frac{L v_x}{D_m};\ \ Pe_p = \frac{L v_x}{D_p};\ \ K_2 = \frac{k_2 c_m^0 L}{v_x};\ \ \Delta = \frac{d}{L}, \end{aligned} \tag{8}$$

where Pe_m and Pe_p are the Péclet numbers associated with the mediator and protein respectively, one can write the normalized mathematical model of the problem as:

$$\begin{aligned} \frac{\partial C_m}{\partial \tau} &= \frac{1}{Pe_m}\frac{\partial^2 C_m}{\partial X^2} - \frac{\partial C_m}{\partial X} - nK_2 C_m C_p;\\ \frac{\partial C_p}{\partial \tau} &= \frac{1}{Pe_p}\frac{\partial^2 C_p}{\partial X^2} - \frac{\partial C_p}{\partial X} - K_2 C_m C_p, \end{aligned} \tag{9}$$

with the corresponding dimensionless initial and boundary conditions:

$$\begin{aligned} \tau = 0\colon \quad & \forall X, && C_m = 1;\\ & X \notin \left[-\frac{\Delta}{2};\ \frac{\Delta}{2}\right], && C_p = 0;\\ & -\frac{\Delta}{2} \le X \le \frac{\Delta}{2}, && C_p = \gamma;\\ \tau > 0\colon \quad & X \to -\infty, && C_m \to 1;\ C_p \to 0;\\ & X \to \infty, && C_m \to 1;\ C_p \to 0. \end{aligned} \tag{10}$$

2.3 Time-dependent coordinate transformation

In current practice the channel length of interest needs to be of the order of several millimeters due to slow reactant/protein kinetics [9, 10], while protein samples widths are of the order of several tens of microns [1, 3, 9, 10]. Therefore, the utilization of a uniform grid along the whole kinetic chamber would be prohibitive for treating the problem. Indeed, this would lead to extremely slow converging and exceedingly time-consuming numerical results. In order to overcome this difficulty we introduce the following time-dependent change of variable:

$$Y = \frac{1}{2} + \frac{1}{\pi}\arctan\left[b\,(X - \tau)\right], \tag{11}$$

where b is a compression coefficient, the choice of which will be discussed below. Since the dimensionless flow rate is equal to unity by definition (see (7)) it is clear from (9) that the origin of the Y space always coincides with the center of the protein sample so that the local grid compression moves along with the protein sample, i.e. is displayed only where it is necessary at any given time (Fig. 2).

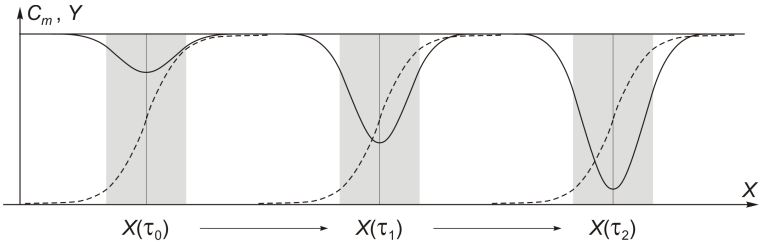

Fig. 2. Schematic displacement of the protein wave (shaded areas) and of the mediator depletion area (solid curves) along the channel with time. The corresponding displacement and modification of space compression is indicated by the dashed lines.

The value of the parameter b is chosen as follows. One would like the grid resolution to be better at the location of the protein sample. This implies that at any time, the transition zone of the arctangent function (viz., the zone around $X - \tau = 0$) covers the whole region where the mediator concentration differs from its steady state value in the absence of a protein wave. Since the protein has a very small diffusivity as compared to the mediator, the half-width of the zone of interest at a given time t_e is at maximum equal to $d_{dif} = d/2 + 2\sqrt{D_m t_e}$.

The space transformation is time-dependent and always centered at the protein sample maximum, so that one may substitute $(X - \tau)$ by d_{dif}/L and derive b from (9) as:

$$b = \frac{L}{d_{dif}} \tan\big(\pi[Y_c - 0.5]\big), \tag{12}$$

where Y_c is the value taken to define the edge of the zone of interest. In our computations we used the value $Y_c = 3/4$ which, upon remarking that $2 \times (3/4 - 1/2) = 1/2$, shows that in the transformed space the zone of main interest occupies half of the overall computational space whose dimensionless length is equal to unity by construction.

Substitution of variables leads to the time-dependent coordinate formulation of the problem:

$$\begin{aligned}\frac{\partial C_m}{\partial \tau} &= S_m(Y)\frac{\partial^2 C_m}{\partial Y^2} + F_m(Y)\frac{\partial C_m}{\partial Y} - nK_2 C_m C_p;\\ \frac{\partial C_p}{\partial \tau} &= S_p(Y)\frac{\partial^2 C_p}{\partial Y^2} + F_p(Y)\frac{\partial C_p}{\partial Y} - K_2 C_m C_p,\end{aligned} \tag{13}$$

with

$$S_j(Y) = \frac{b^2}{\pi^2\, Pe_j}\sin^4(\pi Y); \quad F_j(Y) = \frac{b^2}{\pi Pe_j}\sin(2\pi Y)\sin^2(\pi Y), \tag{14}$$

where $j = m$ or p. The detailed derivation of (13) is given in the Appendix.

The initial and boundary conditions become:

$$\begin{array}{lll}\tau = 0\text{:} & 0 \le Y \le 1, & C_m = 1;\\ & Y \notin \left[\dfrac{1-\Delta_Y}{2};\ \dfrac{1+\Delta_Y}{2}\right], & C_p = 0;\\ & \dfrac{1-\Delta_Y}{2} \le Y \le \dfrac{1+\Delta_Y}{2}, & C_p = \gamma;\\ \tau > 0\text{:} & Y = 0, & C_m = 1;\ C_p = 0;\\ & Y = 1, & C_m = 1;\ C_p = 0,\end{array} \tag{15}$$

where $\Delta_Y = 1/2 + (1/\pi)\arctan(b\,\Delta/2)$.

2.4 Response characteristics and dimension analysis

The kinetics occurring within the homogeneous reaction chamber affects the concentration profiles of the species, resulting in an inverted Gaussian-like shaped concentration profile for the reactant species (Fig. 3). This time-moving Gaussian-shaped profile centered onto the moving protein distribution causes ultimately a time-dependent change in ϕ_{coll} when it passes in front of the collector. In order to obtain a detectable current deviation at the collector electrode we need to optimize some of the parameters of the experiment. Two main (dimensionless) parameters describing the mediator concentration profile indent at the end of the kinetic chamber are its maximum relative amplitude, $\Delta C_m = \Delta c_m / c_m^0$, and its half-width, δ/Δ, relative to that of the protein, Δ (see Fig. 3). It is clear that in order

to extract reliable data ΔC_m should be not too small compared to the background noise. On the other hand, ΔC_m should not reach its maximum value of unity, since this would correspond to a complete titration of the mediator before reaching the end of the kinetic chamber. Would it be the case only a lower bound of the protein quantity may be determined. The closeness of the parameter δ/Δ to unity reflects the fact that the electrochemical detection tracks adequately the shape of the protein sample at the issue of the separating device, viz., at the entrance of the detection system.

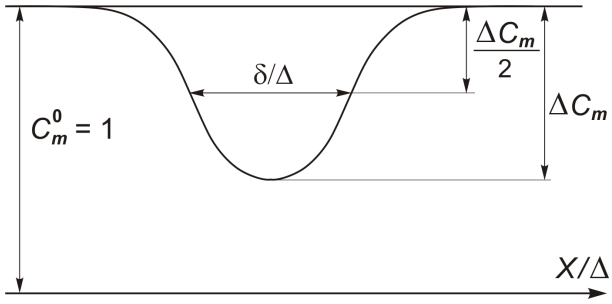

Fig. 3. Definition of the relative time-moving perturbation of the mediator concentration profile (ΔC_m) due to the reaction with the moving protein wave.

The described above analysis of the problem allows us to express these main response characteristics as functions of the dimensionless parameters:

$$\Delta C_m = f(Pe_m, K_2, Pe_m/Pe_p, \gamma, \Delta, n); \tag{16}$$

$$\delta/\Delta = g(Pe_m, K_2, Pe_m/Pe_p, \gamma, \Delta, n), \tag{17}$$

where $Pe_m/Pe_p = D_p/D_m$.

It is evident that even with the assumptions made earlier our system has six degrees of freedom. In order to analyze the system behavior we thus rely on the working surface approach. However, since the number of parameters is still too high to discuss them all here, we will present working surfaces for fixed values of certain parameters based on usual practice in microfluidic channel devices.

3 Results and discussions

First, we wish to extract the dependence of the response characteristics on Pe_m and K_2, since both feature key parameters which can be most easily adjusted experimentally. To this end we fixed the other parameters at the following realistic values: $Pe_m/Pe_p = 5 \times 10^{-3}$ (which corresponds to typical values $D_p = 5 \times 10^{-8}$ cm^2 s^{-1} and $D_m = 10^{-5}$ cm^2 s^{-1}), $\gamma = 1$, $\Delta = 1.2 \times 10^{-2}$ (corresponding to $d = 60$ μm and $L = 5$ mm) and $n = 1$.

Figure 4 shows working surfaces for ΔC_m and δ/Δ as functions of Pe_m

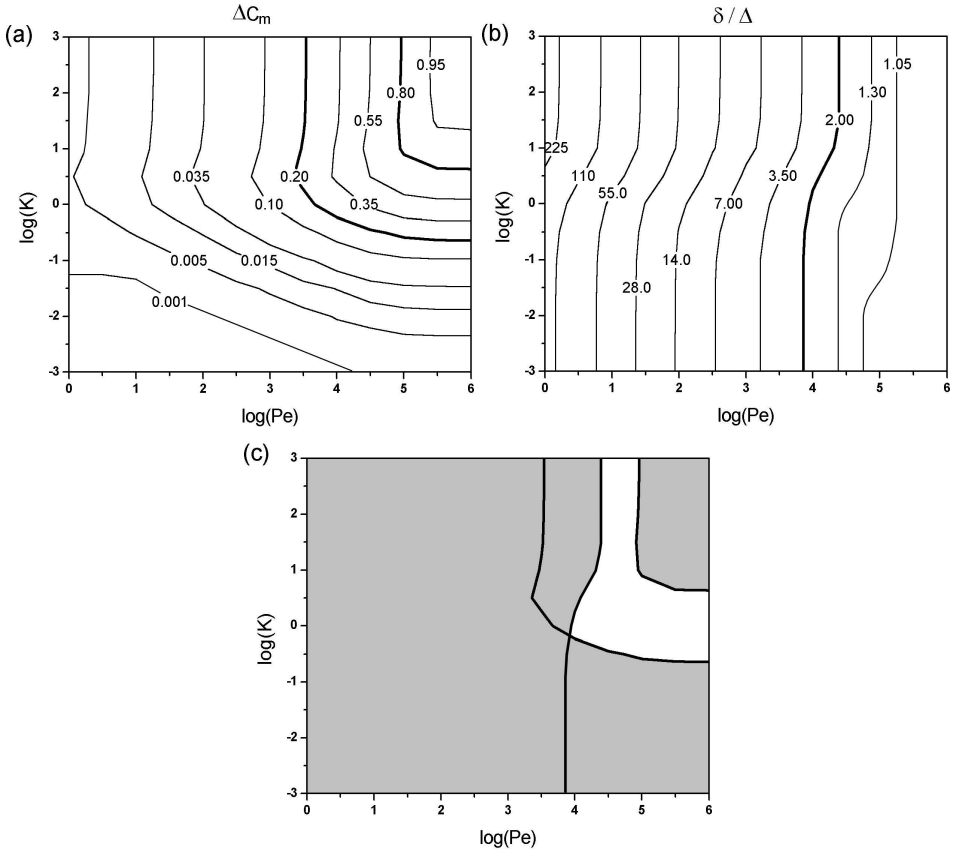

Fig. 4. Working surfaces as functions of K_2 and Pe for: (a) ΔC_m; (b) δ/Δ for parameters: $Pe_m/Pe_p = 5 \times 10^{-3}$, $\gamma = 1$, $\Delta = 1.2 \times 10^{-2}$, $n = 1$. Figure (c) shows the superposition of the constraints $0.2 \leq \Delta C_m \leq 0.8$ and $\delta/\Delta \leq 2$, to define the optimal working area (white area) for this set of conditions.

(hereafter noted Pe for simplification) and K_2. It can be easily identified from both Fig. 4(a) and Fig. 4(b) that the area of best experimental conditions (i.e., $\Delta C_m \to 1$, and $\delta/\Delta \to 1$) lies in the right upper corner, since this corresponds to a sufficiently high deviation of the mediator concentration along with a sufficiently small loss of resolution due to the stretching of the mediator concentration perturbation profile. However, the top right-most area corresponds to high flow rates and high rate constants which are expected not to be achievable as was discussed above. So in order to delineate the optimal working area we proceed as follows. It was explained why the deviation in mediator concentration should not be too small (nearly zero) or too high (close to the bulk mediator concentration). Therefore we select the zone comprised between the lines which represent 20% deflection from these limiting cases (Fig. 4(a)), and posit the delineated range of parameters as belonging to the *optimal detection area*. However, since any important stretching of the mediator concentration deflection profile is detrimental (since this would blur the detection of different proteins), we impose simultaneously that $\delta/\Delta \leq 2$. This creates an additional constraint (Fig. 4(b)) resulting in a more restricted range of parameters for sensitive detection. Superimposition of the two patterns in Fig. 4(a) and Fig. 4(b) defines the optimal detecting zone sketched in Fig. 4(c).

In order to obtain more information about the behavior of the system in this optimal domain of $\log K_2$ and $\log Pe$, we investigated the dynamics of the response as a function of the ratio of the protein and mediator concentrations, γ, but keeping $n = 1$. For this purpose we fixed the lowest Péclet number available from the optimal region obtained from Fig. 4(c), viz. $Pe = 10^4$, and evaluated ΔC_m and δ/Δ as functions of K_2 and γ (Fig. 5). For the same reasons as before, we pick out the zone with deviation of the mediator concentration from 20% up to 80% in Fig. 5(a). The intersection of this zone with that defined by the inequality $\delta/\Delta \leq 2$ in Fig. 5(b) defines now the best zone for the detection in the $(K_2,\ \gamma)$-domain (white area in Fig. 5(c)).

The working surfaces in Fig. 5 are presented as functions of the dimensionless concentration ratio γ and therefore are virtually valid for any values of the protein and mediator concentrations. However, to lead to accurate measurements of ΔC_m, the experimental amplitude of the current measured at the collector in the absence of protein should exceed that of the background noise at least by an order

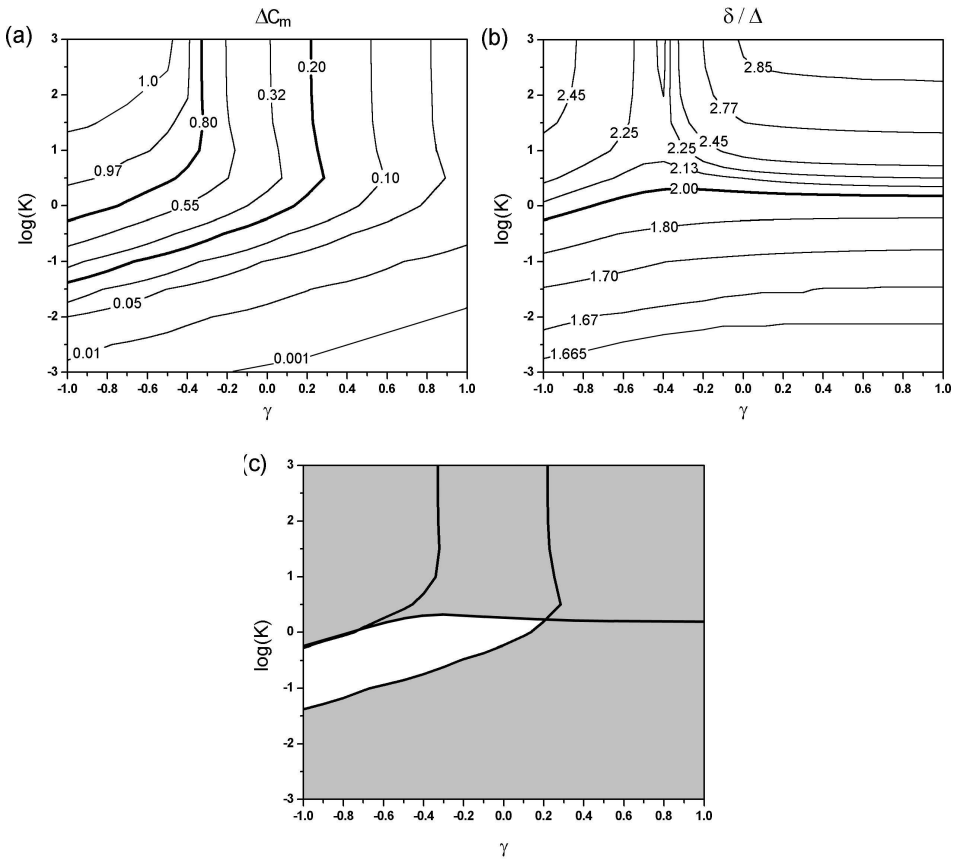

Fig. 5. Working surfaces as functions of K_2 and γ for: (a) ΔC_m; (b) δ/Δ for parameters: $Pe_m/Pe_p = 5 \times 10^{-3}$, $Pe_m = 10^4$, $\Delta = 1.2 \times 10^{-2}$, $n = 1$. Figure (c) shows the superposition of the constraints $0.2 \leq \Delta C_m \leq 0.8$ and $\delta/\Delta \leq 2$, to define the optimal working area (white area) for this set of conditions.

of magnitude. Hence the mediator should be present in the solution at a sufficient concentration. On the other hand, the protein peak concentration will follow from the case at hand, since it depends on availability, sampling, treatment, separation, etc. This implies that for any given set of experimental conditions one would have an additional constraint (which can be computed with the aid of numerical simulation within the generator compartment) which limits the area of optimal conditions, e.g. $\gamma > \gamma_{min}$.

It should be noted that the working surfaces depicted in Fig. 5 were evaluated upon considering the lowest possible Péclet number based on the analysis presented in Fig. 4(c). Identical analyses may be performed for any higher Péclet number to define similar working surfaces indicating similar behavior of the system, yet with different optimal detection zones.

The analyses shown in Fig. 4 and Fig. 5 have been performed for $n = 1$. The same reasoning may be extended to any other n value. For example, the working surfaces for $n = 5$ are displayed in Fig. 6 and Fig. 7, other parameter values being

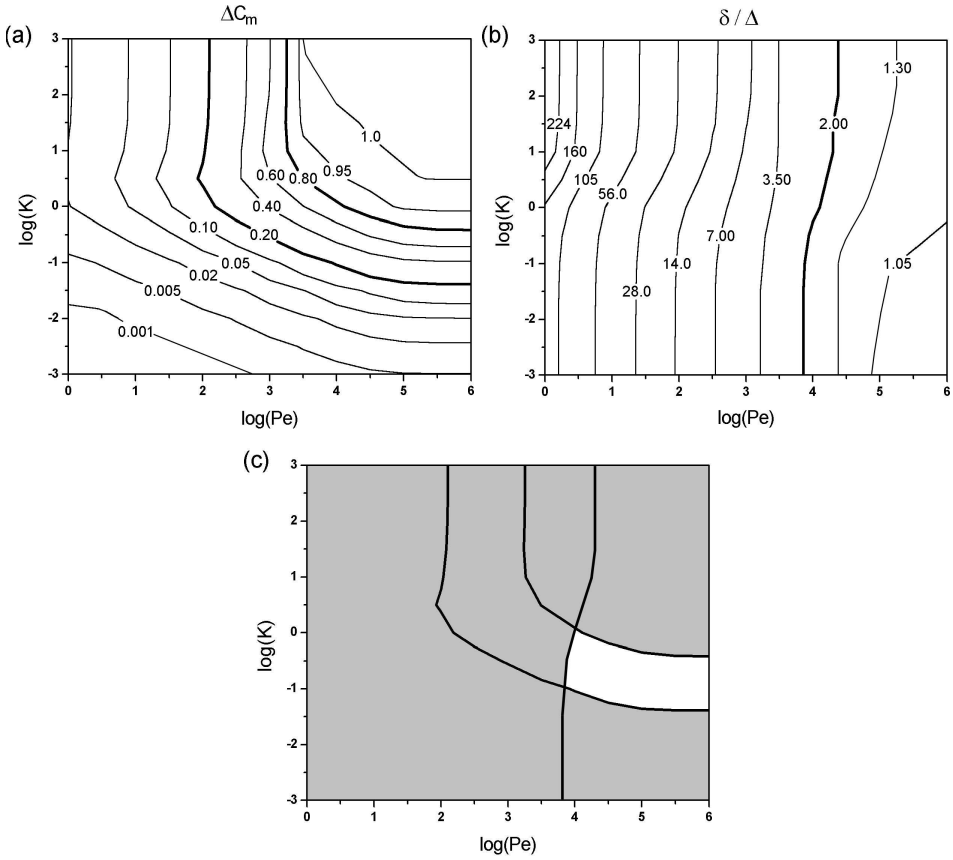

Fig. 6. Working surfaces as functions of K_2 and Pe for: (a) ΔC_m; (b) δ/Δ for parameters: $Pe_m/Pe_p = 5\times10^{-3}$, $\gamma = 1$, $\Delta = 1.2\times10^{-2}$, $n = 5$. Figure (c) shows the superposition of the constraints $0.2 \leq \Delta C_m \leq 0.8$ and $\delta/\Delta \leq 2$, to define the optimal working area (white area) for this set of conditions.

as for Figs. 4, 5. The overall system behavior and optimal domain shapes do not change, but the optimal zones boundaries shift leading to different conditions for optimal detection.

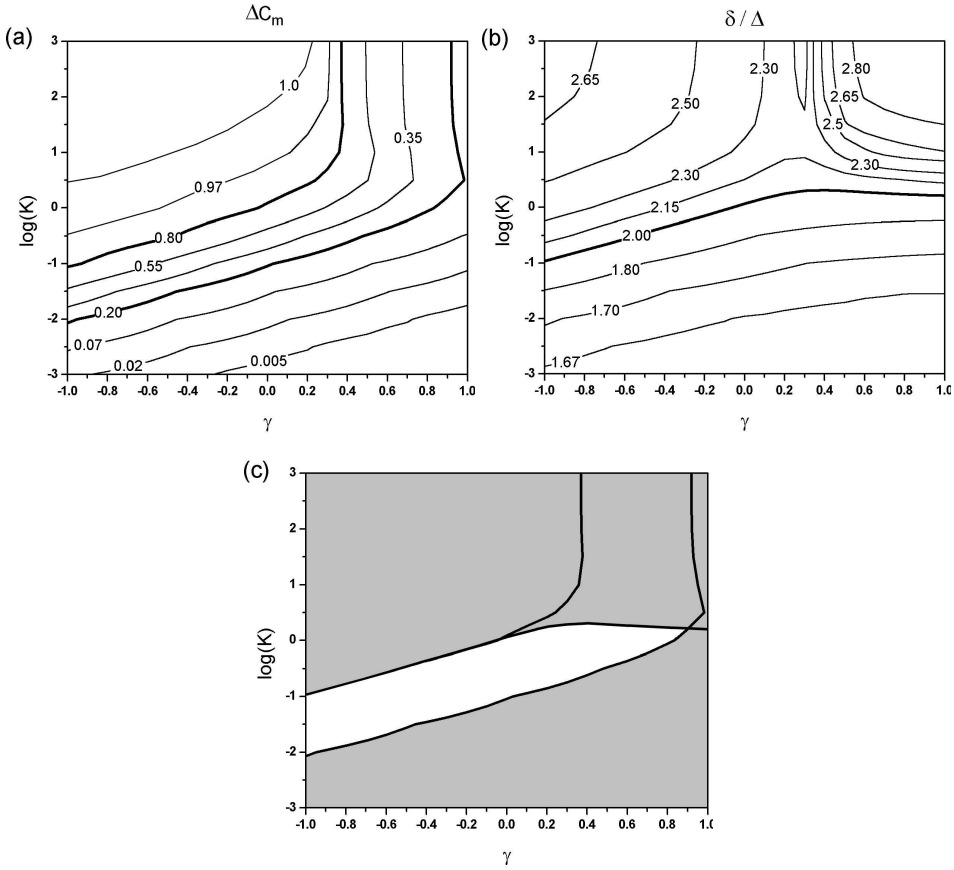

Fig. 7. Working surfaces as functions of K_2 and γ for: (a) ΔC_m; (b) δ/Δ for parameters: $Pe_m/Pe_p = 5 \times 10^{-3}$, $Pe_m = 10^4$, $\Delta = 1.2 \times 10^{-2}$, $n = 5$. Figure (c) shows the superposition of the constraints $0.2 \leq \Delta C_m \leq 0.8$ and $\delta/\Delta \leq 2$, to define the optimal working area (white area) for this set of conditions.

4 Conclusion

The mathematical model of diffusion-convection-reaction processes occurring in microfluidic channels with two band microelectrodes and its solution by an orig-

inal numerical approach justify a novel concept of electrochemical protein detection. To overcome the extremely low diffusivity and generally sluggish electroactivity of proteins, it is proposed to rely on the in-situ electrochemical generation of a fast diffusing reactant able to span across the whole channel so that it may react in extenso with any protein wave transiting into the channel detector. Whenever this fast diffusing reactant is electrochemically collected downstream, any time-dependent change of its collection efficiency is a direct quantitative measurement of the protein wave presence, duration and quantity.

Despite the fact that realistic model simplifications were made to simplify the presentation of our concept and its theoretical analysis, the system possesses in truth many degrees of freedom which shows that a proper analysis will be required for the optimisation of the device. For this purpose the working surface approach used here for defining the range of the physico-chemical parameters corresponding to better detection conditions appears extremely appropriate.

Acknowledgement

In Paris, this work was supported in part by ENS, UPMC, CNRS, and the French Ministry of Research (UMR 8640 and SFR des Sciences Chimiques de l'Analyse et de la Mesure de Paris-Centre, FR CNRS 2702). In Kharkov, this work is a part of research subject 194-1 supported by the Ukrainian Ministry of Science and Education. Dr. Oleinick thanks the Mairie de la Ville de Paris for the one-year post-doctoral fellowship at Ecole Normale Superieure (ENS).

Appendix

Here we present the derivation of the mass-transport equation for the mediator species (13), since the equation for the protein is the same except for the kinetic term which is independent of the coordinate system used. The initial equation in the dimensionless terms is given by (9). Performing the transformation (11), recall that

$$C_m = C_m(Y,\ \tau') = C_m\big(Y[X,\ \tau],\ \tau'\big), \tag{A1}$$

so that the partial derivatives with respect to τ and X rewrite in the following way:

$$\frac{\partial C_m}{\partial \tau} = \frac{\partial C_m}{\partial Y}\frac{\partial Y}{\partial \tau} + \frac{\partial C_m}{\partial \tau'}\frac{\partial \tau'}{\partial \tau} = \frac{\partial C_m}{\partial \tau'} - \frac{b}{\pi\left[1 + b^2(X-\tau)^2\right]}\frac{\partial C_m}{\partial Y}, \quad \text{(A2)}$$

$$\frac{\partial C_m}{\partial X} = \frac{\partial C_m}{\partial Y}\frac{\partial Y}{\partial X} = \frac{b}{\pi\left[1 + b^2(X-\tau)^2\right]}\frac{\partial C_m}{\partial Y}, \quad \text{(A3)}$$

$$\begin{aligned}\frac{\partial^2 C_m}{\partial X^2} &= \frac{\partial^2 C_m}{\partial Y^2}\left(\frac{\partial Y}{\partial X}\right)^2 + \frac{\partial C_m}{\partial Y}\frac{\partial^2 Y}{\partial X^2} \\ &= \frac{b^2}{\pi^2[1 + b^2(X-\tau)^2]^2}\frac{\partial^2 C_m}{\partial Y^2} - \frac{2b^3(X-\tau)}{\pi[1 + b^2(X-\tau)^2]^2}\frac{\partial C_m}{\partial Y}. \quad \text{(A4)}\end{aligned}$$

Next, we express all the coefficients in (A2)–(A4) in terms of the new variables as follows from (11):

$$b(X-\tau) = \tan\left[\pi(Y-0.5)\right] = -\cot(\pi Y), \quad \text{(A5)}$$

$$1 + b^2(X-\tau)^2 = 1 + \cot^2(\pi Y) = \sin^{-2}(\pi Y). \quad \text{(A6)}$$

Substituting the latter into equation (9) yields:

$$\begin{aligned}\frac{\partial C_m}{\partial \tau'} &= \frac{b^2}{\pi^2 Pe_m}\sin^4(\pi Y)\frac{\partial^2 C_m}{\partial Y^2} \\ &\quad + \left[\frac{2b^2}{\pi Pe_m}\cot(\pi Y)\sin^4(\pi Y)\right]\frac{\partial C_m}{\partial Y} - nK_2 C_m C_p.\end{aligned} \quad \text{(A7)}$$

Omitting the stroke for the sake of simplicity and making some simplifications we arrive at the final equation:

$$\begin{aligned}\frac{\partial C_m}{\partial \tau} &= \frac{b^2}{\pi^2 Pe_m}\sin^4(\pi Y)\frac{\partial^2 C_m}{\partial Y^2} \\ &\quad + \frac{b^2}{\pi Pe_m}\sin(2\pi Y)\sin^2(\pi Y)\frac{\partial C_m}{\partial Y} - nK_2 C_m C_p.\end{aligned} \quad \text{(A8)}$$

References

1. N. Lion, T. C. Rohner, L. Dayon, I. L. Arnaud, E. Damoc, N. Youhnovski, Z.-Y. Wu, C. Roussel, J. Josserand, H. Jensen, J. S. Rossier, M. Przybylski, H. H. Girault, Review. Microfluidic systems in proteomics, *Electrophoresis*, **24**(21), pp. 3533–3562, 2003.

2. K. Huikko, R. Kostiainen, T. Kotiaho, Review. Introduction to micro-analytical systems: bioanalytical and pharmaceutical applications, *Eur. J. Pharm. Sci.*, **20**(2), pp. 149–171, 2003.

3. M. Lazar, J. Grym, F. Foret, Review. Microfabricated devices: A new sample introduction approach to mass spectrometry, *Mass Spectrom. Rev.*, **25**(4), pp. 573–594, 2006.

4. A. J. Bard, M. Stratmann, Chapters 1, 14, 17, in: *Encyclopedia of Electrochemistry: Bioelectrochemistry,* Vol. 9, G. S. Wilson (Ed.), Wiley-VCH, 2002.

5. C. Amatore, M. Belotti, Y. Cheng, E. Roy, C. Sella, L. Thouin, Using electrochemical coupling between parallel microbands for in situ monitoring of flow rates in microfluidic channels, *J. Electroanal. Chem.*, **573**(2), pp. 333–343, 2004.

6. C. Amatore, C. Sella, L. Thouin, Electrochemical time-of-flight responses at double-band generator-collector devices under pulsed conditions, *J. Electroanal. Chem.*, **593**(1–2), pp. 194–202, 2006.

7. R. S. Martin, A. J. Gawron, S. M. Lunte, C. S. Henry, Dual-electrode electrochemical detection for poly(dimethylsiloxane)-fabricated capillary electrophoresis microchips, *Anal. Chem.*, **72**(14), pp. 3196–3202, 2000.

8. R. G. Compton, B. A. Coles, J. J. Gooding, A. C. Fisher, T. I. Cox, Chronoamperometry at Channel Electrodes: Experimental Applications of Double Electrodes, *J. Phys. Chem.*, **98**(9), pp. 2446–2451, 1994.

9. T. C. Rohner, J. S. Rossier, H. H. Girault, On-line electrochemical tagging of cysteines in proteins during nanospray, *Electrochem. Commun.*, **4**(9), pp. 695–700, 2002.

10. C. Roussel, T. C. Rohner, H. Jensen, H. H. Girault, Mechanistic Aspects of On-Line Electrochemical Tagging of Free L-Cysteine Residues during Electrospray Ionisation for Mass Spectrometry in Protein Analysis, *ChemPhysChem*, **4**(2), pp. 200–206, 2003.

11. C. Amatore, O. Klymenko, I. Svir, In situ and on-line monitoring of hydrodynamic flow profiles in microfluidic channels based upon microelectrochemistry: Optimisation of electrode locations, *ChemPhysChem*, **7**(2), pp. 482–487, 2006.

12. C. Amatore, A. Oleinick, I. Svir, Simulation of diffusion–convection processes in microfluidic channels equipped with double band microelectrode assemblies: approach through quasi-conformal mapping, *Electrochem. Commun.*, **6**(11), pp. 1123–1130, 2004.

13. J. A. Alden, Compton R.G. Automated Simulation of Electrode Processes: Quantitative Mechanistic Analysis via Working Surface Interpolation, *J. Phys. Chem. B,* **101**(47), pp. 9741–9750, 1997.

14. K. Harriman, D. J. Gavaghan, P. Houston, D. Kay, E. Suli, Adaptive finite element simulation of currents at microelectrodes to a guaranteed accuracy. ECE and EC_2E mechanisms at channel microband electrodes, *Electrochem. Commun.,* **2**(8), pp. 576–585, 2000.

15. T. C. Rohner, J. Josserand, H. Jensen, H. H. Girault, Numerical Investigation of an Electrochemically Induced Tagging in a Nanospray for Protein Analysis, *Anal. Chem.,* **75**(9), pp. 2065–2074, 2003.

16. L. Dayon, J. Josserand, H. H. Girault, Electrochemical multi-tagging of cysteinyl peptides during microspray mass spectrometry: numerical simulation of consecutive reactions in a microchannel, *Phys. Chem. Chem. Phys.,* **7**(24), pp. 4054–4060, 2005.

17. V. G. Levich, *Physico-chemical hydrodynamics,* Academy of Sciences of USSR, Moscow, 1952.

18. L. D. Landau, E. M. Lifshitz, *Theoretical physics. Hydrodynamics,* Science, Moscow, 1988.

19. C. Amatore, A. Oleinick, O. V. Klymenko, I. Svir, In situ and online monitoring of hydrodynamic flow profiles in microfluidic channels based upon microelectrochemistry: Concept, theory, and validation, *ChemPhysChem,* **6**(8), pp. 1581–1589, 2005.

20. P. G. de Gennes, On fluid/wall slippage, *Langmuir,* **18**(9), pp. 3413–3414, 2002.